Desalination and Water Treatment
www.deswater.com
doi: 10.1080/19443994.2015.1038589

57 (2016) 10757–10766
May

Taylor & Francis
Taylor & Francis Group

Functionalization of activated carbon fiber through iron oxide impregnation for As(V) removal: equilibrium, kinetic, and thermodynamic analyses

In Lee[a], Jeong-Ann Park[a], Jae-Hyun Kim[a], Jin-Kyu Kang[a], Chang-Gu Lee[b], Song-Bae Kim[a,c,*]

[a]*Environmental Functional Materials and Biocolloids Laboratory, Seoul National University, Seoul 151-921, Republic of Korea, Tel. +82 2 880 4595; emails: usquebaugh@snu.ac.kr (I. Lee), pjaan720@snu.ac.kr (J.-A. Park), kjh85@snu.ac.kr (J.-H. Kim), naengie@snu.ac.kr (J.-K. Kang), Tel. +82 2 880 4587; Fax: +82 2 873 2087; email: songbkim@snu.ac.kr (S.-B. Kim)*
[b]*Center for Water Resource Cycle Research, Korea Institute of Science and Technology, Seoul 136-791, Republic of Korea, Tel. +82 2 880 4595; email: changgu@kist.re.kr*
[c]*Department of Rural Systems Engineering and Research Institute of Agriculture and Life Sciences, Seoul National University, Seoul 151-921, Republic of Korea*

Received 17 March 2014; Accepted 29 March 2015

ABSTRACT

The aim of this study was to investigate the removal of As(V) from aqueous solutions using functionalized activated carbon fiber (ACF) as an adsorbent. The functionalized ACF was prepared through the impregnation of iron oxides on the surfaces of ACF. The X-ray fluorescence spectrometer analysis showed that carbon (C, 70.1%) and iron (Fe, 28.5%) were the major constituents of functionalized ACF. The N_2 adsorption–desorption analysis showed that the Brunauer–Emmett–Teller surface area of functionalized ACF was determined to be 418.2 m^2/g, which was 2.7 times smaller than that of raw ACF (1,123.0 m^2/g) due to the impregnation of iron oxide. From the batch experiments, the maximum adsorption capacity of As(V) in functionalized ACF was determined to be 1.208 mg/g. The adsorption of As(V) to functionalized ACF was sensitive to solution pH changes, decreasing from 0.045 to 0.029 mg/g with increasing pH from 2.6 to 8.9. Kinetic model analysis showed that the pseudo-second-order model was most suitable at describing the kinetic data. Equilibrium isotherm model analysis illustrated that the Redlich–Peterson model fitted well with the equilibrium data. Thermodynamic tests demonstrated that As(V) sorption to functionalized ACF increased with increasing temperature from 20 to 40°C, indicating the endothermic and spontaneous nature of sorption process (ΔH° = 38.02 kJ/mol, ΔS° = 149.15 J/K/mol, and ΔG° = –5.70 and –8.69 kJ/mol). This study demonstrated that the removal of As(V) by ACF could be enhanced via iron oxide impregnation.

Keywords: Activated carbon fiber; Adsorption; Arsenic removal; Functionalization; Iron oxide impregnation

*Corresponding author.

1. Introduction

Arsenic is the major contaminant found in water environments. In many countries such as Bangladesh, Chile, and India, arsenic occurs naturally in groundwater at concentrations exceeding 10 μg/L (guideline of World Health Organization, 2000), causing serious health-related problems and human mortality [1]. Arsenic exists in nature as As(III) (arsenite) and As(V) (arsenate) depending on the redox conditions. Under oxidizing environments, As(V) is predominant while As(III) occurs under reducing conditions. As(III) is known to be more toxic and mobile than As(V) [2].

Activated carbon fiber (ACF) is a kind of activated carbons, which is used extensively as an adsorbent. It is synthesized through two-step processes of carbonization followed by activation using source materials such as cellulose, phenolic resin, pitch, and polyacrylonitrile. ACF has thin-fiber shape with a diameter of 10 μm and contains inner porous network of mesopores and micropores [3]. It is widely applied for water purification because of fast intraparticle adsorption compared with powdered and granular forms of activated carbon [4]. ACF has been investigated for the removal of contaminants such as heavy metals, organic compounds, and oxyanions by several researchers [5,6].

The functionalization of ACF through the impregnation of various functional materials (silver, copper, titanium dioxide, lanthanum oxide, iron oxide, etc.) has been performed by many researchers to enhance the adsorption of specific contaminants or removal of microorganisms [7–9]. For instance, Chui et al. [10] loaded palladium onto ACF to remove pentachlorophenol from aqueous solutions through electrocatalytic dechlorination. Shi et al. [11] immobilized titanium dioxide on ACF and observed the photocatalytic degradation of dyes such as methyl orange and acid fuchsine. Kim and Park [12] prepared copper- or silver-plated ACF and examined their antibacterial behavior against *Staphylococcus aureus* and *Klebsiella pneumonia*. Liu et al. [13] used lanthanum-doped ACF to adsorb phosphate from aqueous solutions. However, very few studies have been performed using functionalized ACF as an adsorbent to remove arsenic from aqueous solutions. Hristovski et al. [14] modified ACF with iron (hydr)oxide using two synthesis methods (aqueous $KMnO_4$ pretreatment plus Fe(II) treatment, reaction with Fe(III) in an organic solvent plus NaOH treatment). They performed the batch experiment to remove arsenate from water and to determine the arsenate adsorption capacity of the modified ACF. Zhang et al. [15,16] prepared magnetite-doped ACF to enhance arsenic removal and studied the mechanisms of arsenate adsorption using X-ray photoelectron spectroscopy. They showed that the As(V) adsorption capacity of magnetite-doped ACF was about eight times larger than that of raw ACF.

The objective of study was to analyze the equilibrium, kinetic, and thermodynamics of the adsorptive As(V) removal from aqueous solutions using functionalized ACF as an adsorbent. Functionalized ACF was prepared through the impregnation of iron oxides on the surfaces of ACF. The characteristics of ACF were elucidated using field emission scanning electron microscopy (FESEM), X-ray fluorescence (XRF) spectrometer, X-ray diffractometry (XRD), Fourier transform infrared (FTIR) spectrometer, and nitrogen gas (N_2) adsorption–desorption experiment. Batch experiments were performed to examine the effects of reaction time, temperature, As(V) concentration, and solution pH on the removal of As(V) by functionalized ACF. In addition, kinetic, equilibrium isotherm, and thermodynamic models were used to analyze the experimental data.

2. Materials and methods

2.1. Preparation of functionalized ACF

All chemicals were purchased from Sigma-Aldrich. In addition, cotton-based ACF was obtained from Korea Activated Carbon Fiber Ltd. In the preparation of functionalized ACF, chitosan was used as the coating (film) support for iron oxide impregnation, whereas sodium tripolyphosphate was used as the crosslinking agent for chitosan film formation [17]. The functionalized ACF was prepared through a two-step procedure. First, a suspension of iron oxide particles was prepared by coprecipitating a solution of iron chloride ($FeCl_3{\cdot}6H_2O$) and iron sulfate ($FeSO_4{\cdot}7H_2O$). A solution of sodium hydroxide (NaOH, 6 M) was added drop wise with intensive stirring at room temperature into a 500 mL solution of $FeCl_3{\cdot}6H_2O$ (0.25 mol) and $FeSO_4{\cdot}7H_2O$ (0.125 mol) until pH 8 was reached. The suspension was then aged at 60°C for 24 h and rinsed with deionized water until a neutral pH was reached.

Second, a chitosan solution was prepared by adding 3.0 g of chitosan powder into 600 mL of 1% acetic acid solution. A total of 12 g of raw ACF were soaked in the iron oxide suspension and then oven-dried at 150°C for 6 h. The oven-dried ACF was soaked in the chitosan solution and aged for 12 h. The ACF was soaked again in 300 mL of 1% sodium

tripolyphosphate solution for 1 h. Finally, the functionalized (iron oxide impregnated) ACF was rinsed with deionized water and dried at 60˚C for 12 h prior to use.

2.2. Characterization of functionalized ACF

Various techniques were used to analyze the characteristics of the functionalized ACF. FESEM and energy dispersive X-ray spectrometer (EDS) analyses were performed using a field emission scanning electron microscope (Supra 55VP, Carl Zeiss, Germany). The chemical composition was investigated using an XRF spectrometer (S4 Pioneer, Bruker, Germany). The mineralogical and crystalline structural properties were examined using (XRD, D8 Discover, Bruker, Germany) with a CuKα radiation of 1.5406 Å at a scanning speed of 0.6 ○/sec. Infrared spectra were recorded on a Nicolet 6700 (Thermo Scientific, USA) FTIR spectrometer using KBr pellets. A nitrogen gas (N_2) adsorption–desorption experiments were performed using a surface area analyzer (BELSORP-max, BEL Japan Inc., Japan) after the sample was pretreated at 120˚C. From the N_2 adsorption–desorption isotherms, the specific surface area, average pore diameter, total pore volume, and mesopore volume were determined by Brunauer–Emmett–Teller (BET) and Barrett–Joyner–Halenda analyses.

2.3. Batch experiments

A stock solution of As(V) was prepared by dissolving reagent-grade sodium arsenate ($Na_2HAsO_4{\cdot}7H_2O$) in deionized water. All batch experiments were performed at 30˚C in 50-mL polypropylene conical tubes without pH adjustment unless otherwise stated. All of the batch experiments were performed in triplicate.

The first set of experiments was conducted to examine the effect of reaction time on the removal of As(V) using functionalized ACF. The experiments were conducted at an As(V) concentration of 1 mg/L with a functionalized ACF dose of 1.0 g in a 50 mL solution. Note that the pH of the 1 mg/L As(V) solution was 4.5. The tubes were shaken at 30˚C and 100 rpm using a shaking incubator (Daihan Science, Seoul, Korea). The samples were collected after various reaction times and then filtered through a 0.45 μm membrane filter. Arsenic concentrations were measured by inductively coupled plasma-atomic emission spectroscopy (ICP-AES) (ICP-730 ES, Varian, Australia). Additional experiments were performed at 20 and 40˚C to examine the effect of temperature on As (V) removal with functionalized ACF.

The second set of experiments was performed to observe the effect of the initial As(V) concentration on the removal of As(V) with concentrations ranging from 1 to 50 mg/L (adsorbent dose = 20 g/L; reaction time = 12 h). The third set of experiments was conducted to examine the effect of the solution pH on the removal of As(V) with functionalized ACF (adsorbent dose = 20 g/L; As(V) concentration = 1 mg/L; reaction time = 12 h). In the experiments, 0.1 M NaOH and 0.1 M HCl solutions were used to adjust the pH from 2.6 to 8.9, and the pH was measured by a pH probe (9107BN, Thermo Scientific, USA).

2.4. Data analysis

All of the parameters of the models were estimated using MS Excel 2010 with solver add-in function incorporated into the program. The determination coefficient (R^2), chi-square coefficient (χ^2), and sum of the squared errors (SSE) were used to analyze the data and confirm the fit to the model. The expressions of R^2, χ^2, and SSE are given below:

$$R^2 = \frac{\sum_{i=1}^{m}(y_c - \bar{y}_e)_i^2}{\sum_{i=1}^{m}(y_c - \bar{y}_e)_i^2 + \sum_{i=1}^{m}(y_c - y_e)_i^2} \quad (1)$$

$$\chi^2 = \sum_{i=1}^{m}\left[\frac{(y_e - y_c)^2}{y_c}\right]_i \quad (2)$$

$$\mathrm{SSE} = \sum_{i=1}^{m}(y_e - y_c)_i^2 \quad (3)$$

where y_c is the calculated adsorption capacity from the model, y_e is the measured adsorption capacity from the experiment, and $\bar{y}_e$ is the average of the measured adsorption capacity.

3. Results and discussion

3.1. Characteristics of functionalized ACF

The characteristics of functionalized ACF are presented in Fig. 1. ACF had a thin-fiber shape with a diameter of 10 μm. The iron oxide particles were immobilized on the surfaces of ACF (Fig. 1(a)). From N_2 adsorption–desorption analyses of ACF and functionalized ACF, the BET surface area of ACF was determined to be 1,123.0 m^2/g with a total pore volume of 0.52 cm^3/g, a mesopore volume of 0.09 cm^3/g,

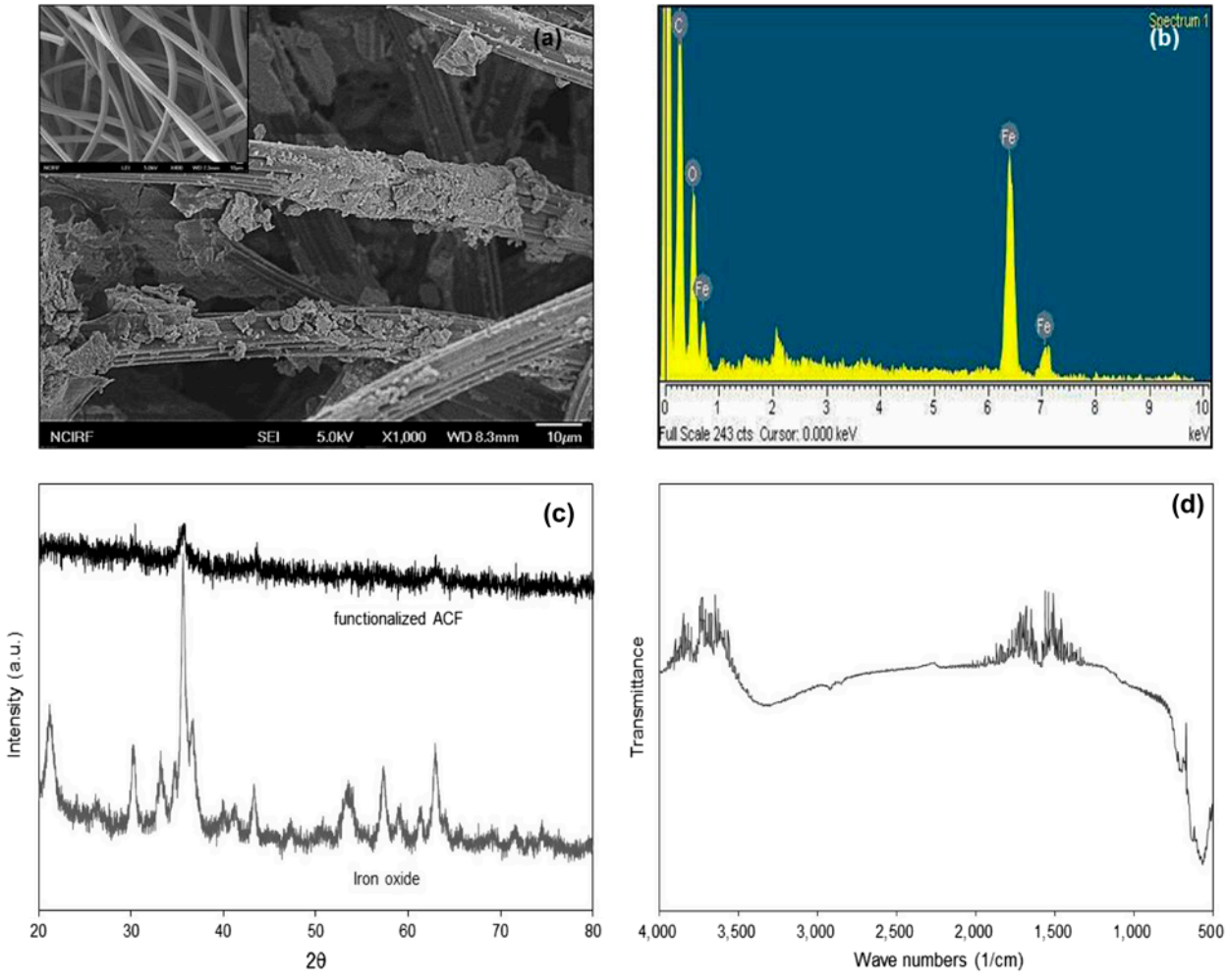

Fig. 1. Characteristics of functionalized ACF: (a) FESEM image (bar = 10 μm; inset = raw ACF), (b) EDS pattern, (c) XRD pattern, and (d) FTIR spectra.

and an average pore diameter of 1.85 nm. In functionalized ACF, the BET surface area was 418.2 m^2/g, which was 2.7 times smaller than that of ACF due to the impregnation of iron oxide. In addition, the total pore volume was reduced to 0.37 cm^3/g. The XRF analysis indicated that carbon (C, 70.1%) and iron (Fe, 28.5%) were the major constituents of functionalized ACF. The EDS pattern (Fig. 1(b)) demonstrated that C and Fe were the major elements of functionalized ACF. Through EDS analysis, C was evident from the peak position of 0.277 keV as the K α X-ray signal, whereas Fe was found at the peak positions of 0.707, 6.403, and 7.057 keV, as the L α, K α, and K β X-ray signals, respectively.

The XRD pattern of iron oxide (Fig. 1(c)) indicated major peaks corresponding to maghemite (γ-Fe_2O_3, JCPDS 89-5892, 2θ = 30.266, 35.651, 43.332, 53.766, 57.319, 62.949) along with goethite peaks (α-FeOOH, JCPDS 81-0464, 2θ = 21.240, 33.243, 41.183, 58.998). The XRD pattern of functionalized ACF showed the major peaks found in the iron oxide (Fig. 1(c)). In the FTIR spectra of functionalized ACF (Fig. 1(d)), two peaks at 2,950 and 2,880 cm^{-1} corresponded to symmetric stretching vibrations of $–CH_2$ and –CH, respectively. In addition, a band corresponding to C=O was observed at 1,680–1,720 cm^{-1} [6]. The bands at 724, 694, 638, 584, and 558 cm^{-1} were attributed to the iron oxides [18].

3.2. Characteristics of As(V) removal by functionalized ACF

The effect of reaction time on the removal of As(V) by functionalized ACF is shown in Fig. 2(a). At 1 h of reaction time, the adsorption capacity was 0.023 mg/g with a percent removal of 48.6%. The adsorption capacity increased to 0.036 mg/g with a percent removal of

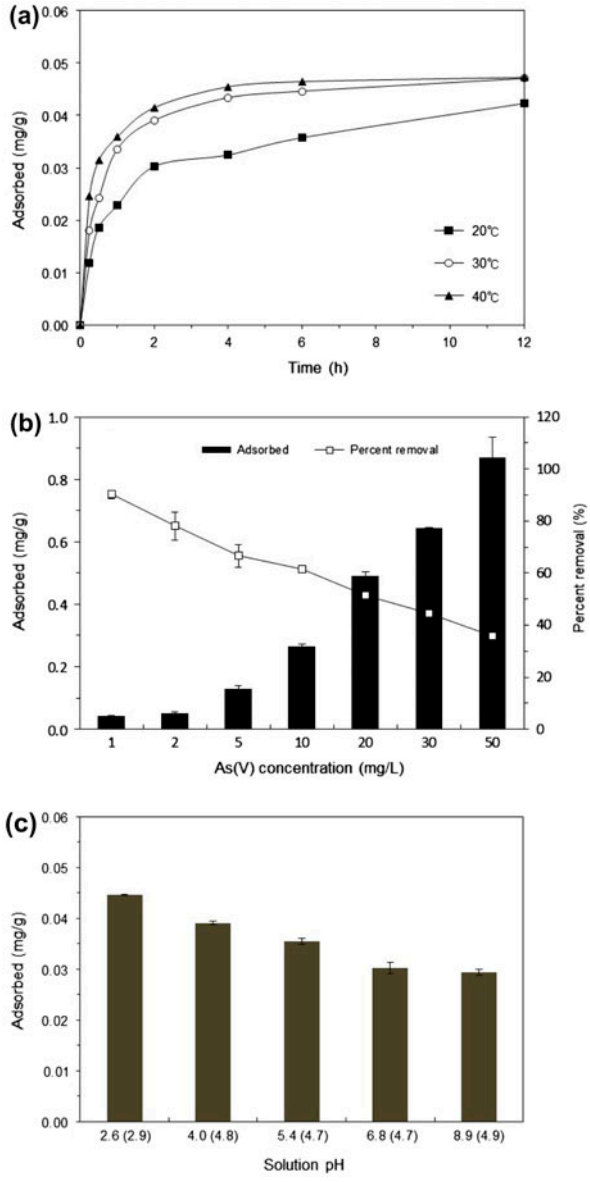

Fig. 2. Removal of As(V) by functionalized ACF: (a) effect of reaction time, (b) effect of As(V) concentration, and (c) effect of solution pH (numbers in the parenthesis of the *x*-axis are final pH).

76.2% at 6 h. At 12 h, the adsorption capacity and percent removal were 0.042 mg/g and 90.2%, respectively. The effect of As(V) concentration on the removal of As (V) by functionalized ACF is presented in Fig. 2(b). At the lowest concentration of 1 mg/L, the adsorption capacity was 0.042 mg/g, while the adsorption capacity increased to 0.871 mg/g at the highest concentration of 50 mg/L. Meanwhile, the percent removal decreased with increasing As(V) concentration. The percent removal was 90.2% at 1 mg/L and decreased to 35.7% at 50 mg/L. It should be noted that the As(V) adsorption capacity of raw ACF at 12 h was negligible, indicating an enhancement of As(V) removal due to the surface modification of ACF by iron oxide impregnation. Arsenic adsorption to iron (hydr)oxides can be described by the ligand exchange mechanism [15,16]. In the adsorption process, arsenic species can replace hydroxyl ion (OH^-) on the surfaces of iron (hydr)oxides, forming inner-sphere complexes. Also, the electrostatic attraction between positively charged iron (hydr) oxides and negatively charged arsenic species can contribute to the removal of As(V). Zhang et al. [15,16] reported that in addition to ligand exchange, the electrostatic interaction contributes to the adsorption of As (V) to magnetite-doped ACF.

The effect of the solution pH on the removal of As (V) by functionalized ACF is demonstrated in Fig. 2(c). As(V) removal decreased with increasing pH. The adsorption capacity at pH 2.6 was 0.045 mg/g. As the solution pH increased to 5.4, the adsorption capacity decreased to 0.035 mg/g. The adsorption capacity approached 0.029 mg/g as the solution pH further increased to 8.9. These results indicated that the removal of As(V) in functionalized ACF was sensitive to changes in the solution pH and became more favorable in an acidic solution pH. The pH dependency of As(V) adsorption to functionalized ACF is primarily related to the ionization of As(V) and the adsorbent in accordance with pH changes. In the pH range between 2.7 and 6.8, $H_2AsO_4^-$ (monovalent anion) is the dominant form of As(V). For pH values of 6.8–11.6, $HAsO_4^{2-}$ (divalent anion) dominates. The point of zero charge (pH_{PZC}) of the iron oxides used for the impregnation of ACF was determined to be 7.6 from the previous study [19]. Below pH_{PZC}, the iron oxide is positively charged, whereas it is negatively charged above pH_{PZC}. Therefore, the adsorption of As(V) is favorable below pH 7.6 due to the electrostatic attraction between As(V) and the iron oxide, even though the percent removal gradually decreased with an increase in the pH. Above pH 7.6, the adsorption of As(V) becomes unfavorable since the electrostatic interaction between As(V) and the iron oxide becomes repulsive [16]. Our results are in agreement with the report of Zhang et al. [15,16], who showed a decrease of As(V) adsorption to magnetite-doped ACF with increasing pH from 3.0 to 11.6.

3.3. Kinetic and intraparticle diffusion model analyses

The reaction time data were analyzed using the following nonlinear forms of pseudo-first-order (Eq. (4)), pseudo-second-order (Eq. (5)), and Elovich (Eq. (6)) kinetic models [20]:

$$q_t = q_e(1 - e^{-k_1 t}) \quad (4)$$

$$q_t = \frac{k_2 q_e^2 t}{1 + k_2 q_e t} \quad (5)$$

$$q_t = \frac{1}{\beta} \ln(\alpha\beta) + \frac{1}{\beta} \ln t \quad (6)$$

where q_t is the amount of As(V) removed at time t, q_e is the amount of As(V) removed per unit mass of adsorbent at equilibrium, k_1 is the pseudo-first-order rate constant, k_2 is the pseudo-second-order velocity constant, α is the initial adsorption rate constant, and β is the Elovich adsorption constant.

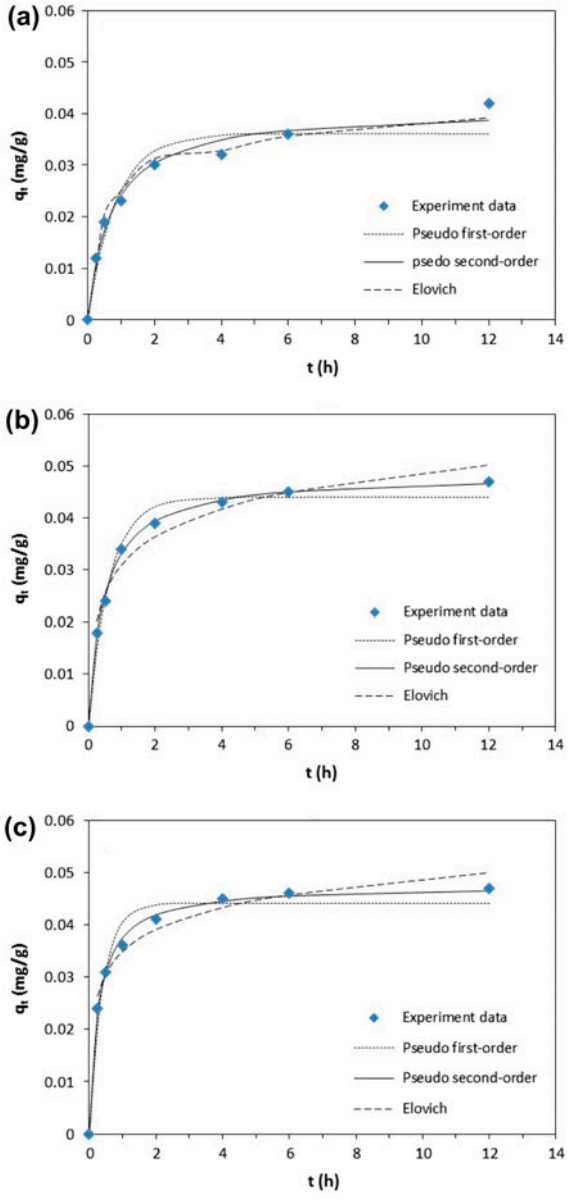

Fig. 3. Kinetic model analysis: (a) 20℃, (b) 30℃, and (c) 40℃. Model parameters are provided in Table 1.

The kinetic data and model fit for As(V) removal with functionalized ACF are shown in Fig. 3. Model parameters for the pseudo-first-order, pseudo-second-order, and Elovich models are provided in Table 1. The values of R^2, χ^2, and SSE indicate that the pseudo-second-order model was the most suitable for describing the data. This finding indicated that chemisorption is involved in the adsorption of As(V) to functionalized ACF. In the pseudo-second-order model, the values of q_e increased from 0.041 to 0.049 mg/g with increasing temperature from 20 to 40℃, demonstrating that the adsorption capacity of As(V) increased with increasing temperature. The value of k_2 also increased from 35.60 to 78.41 g/mg/h with increasing temperature, indicating that the time needed to reach equilibrium decreased with increasing temperature. The initial adsorption rate constant (h) at $t \rightarrow 0$ can be calculated from the rate constant k_2 using the following Eq. (20):

$$h = k_2 q_e^2 \quad (7)$$

The values of h increased with increasing temperature, indicating that the adsorption at an early phase of the sorption process grew faster with increasing temperature. The values of h were lower than the initial adsorption rate constant (α) from the Elovich model.

The kinetic sorption data analyzed by the following intraparticle diffusion model:

$$q_t = K_i t^{1/2} + I \quad (8)$$

where K_i is the intraparticle diffusion rate constant, and I is the intercept related to the thickness of the boundary layer. The intraparticle diffusion model analysis is shown in Fig. 4, indicating that the plots were composed of two line segments. The first line in the plot indicates boundary layer adsorption, while the second line describes the intraparticle diffusion [21]. Model parameters for the intraparticle diffusion model are presented in Table 2. The values of K_i for the first and second lines were 0.0177–0.0233 and 0.0026–0.0060 mg/g/h$^{1/2}$, respectively. The diffusion model was well fitted to the data, with coefficients of determination (R^2) of 0.957–0.977 (first line) and 0.759–0.987 (second line).

Table 1
Kinetic model parameters obtained from model fitting to experimental data

	Pseudo-first-order model					Pseudo-second-order model					Elovich model				
Temp. (°C)	q_e (mg/g)	k_1 (1/h)	R^2	SSE	χ^2	q_e (mg/g)	k_2 (g/mg/h)	h (mg/g/h)	R^2	SSE	χ^2	α (mg/g/h)	β (g/mg)	R^2	SSE	χ^2
20	0.036	1.19	0.942	7.7×10^{-5}	2.8×10^{-3}	0.041	35.60	0.07	0.980	2.6×10^{-5}	8.8×10^{-4}	0.17	135.1	0.989	2.2×10^{-5}	1.0×10^{-3}
30	0.044	1.61	0.981	3.4×10^{-5}	1.2×10^{-3}	0.048	45.11	0.10	0.998	3.0×10^{-6}	1.4×10^{-4}	0.42	128.2	0.951	3.5×10^{-5}	1.1×10^{-3}
40	0.045	2.49	0.967	5.3×10^{-5}	1.5×10^{-3}	0.049	78.41	0.19	0.997	5.0×10^{-6}	1.5×10^{-4}	1.86	163.9	0.949	2.3×10^{-5}	6.0×10^{-4}

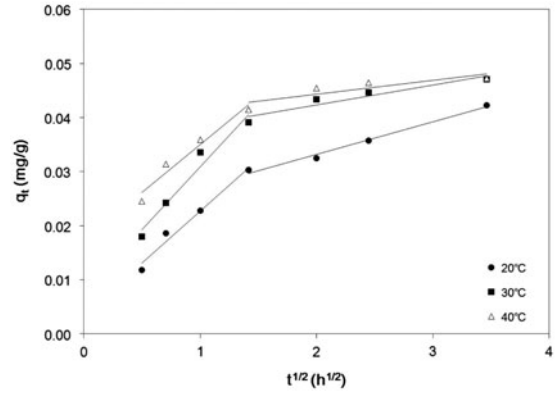

Fig. 4. Intraparticle diffusion model analysis. Model parameters are provided in Table 2.

3.4. Equilibrium model and thermodynamic analyses

The As(V) concentration data were analyzed using the following nonlinear forms of Freundlich (Eq. (9)), Langmuir (Eq. (10)), and Redlich–Peterson (Eq. (11)) isotherm models [22]:

$$q_e = K_F C_e^{1/n} \tag{9}$$

$$q_e = \frac{Q_m K_L C_e}{1 + K_L C_e} \tag{10}$$

$$q_e = \frac{K_R C_e}{1 + a_R C_e^g} \tag{11}$$

where q_e is the amount of As(V) removed at equilibrium (mg/g), C_e is the concentration of As(V) in the aqueous solution at equilibrium, K_F is the distribution coefficient, $1/n$ is the Freundlich constant, Q_m is the maximum mass of As(V) removed per unit mass of adsorbent (removal capacity), K_L is the Langmuir constant related to the binding energy, K_R is the Redlich–Peterson constant related to the adsorption capacity, a_R is the Redlich–Peterson constant related to the affinity of the binding sites, and g is the Redlich–Peterson constant related to the adsorption intensity.

The equilibrium data and isotherm model fits for As(V) removal in functionalized ACF are given in Fig. 5. The equilibrium isotherm parameters are summarized in Table 3. The values of R^2, χ^2, and SSE indicate that the Redlich–Peterson model was the most suitable for describing the data. In the Redlich–Peterson model, the value of K_R was 0.175 L/g, and the value of a_R was 0.524 L/mg. From the Langmuir model, the maximum As(V) adsorption capacity (Q_m)

Table 2
Intraparticle diffusion model parameters obtained from model fitting to experimental data

Temp. (°C)	$K_{i,1}$ (mg/g/h$^{0.5}$)	I	R^2	$K_{i,2}$ (mg/g/h$^{0.5}$)	I	R^2
20	0.0193	0.0034	0.977	0.0060	0.0212	0.987
30	0.0233	0.0076	0.959	0.0037	0.0350	0.906
40	0.0177	0.0173	0.957	0.0026	0.0392	0.759

Table 3
Equilibrium isotherm model parameters obtained from model fitting to experimental data

Freundlich isotherm					Langmuir isotherm					Redlich–Peterson isotherm					
K_F (L/g)	$1/n$	R^2	SSE	χ^2	Q_m (mg/g)	K_L (L/mg)	R^2	SSE	χ^2	K_R (L/g)	a_R (L/mg)	g	R^2	SSE	χ^2
0.140	0.537	0.995	0.0031	0.022	1.208	0.077	0.994	0.0035	0.045	0.175	0.524	0.671	0.998	0.0010	0.021

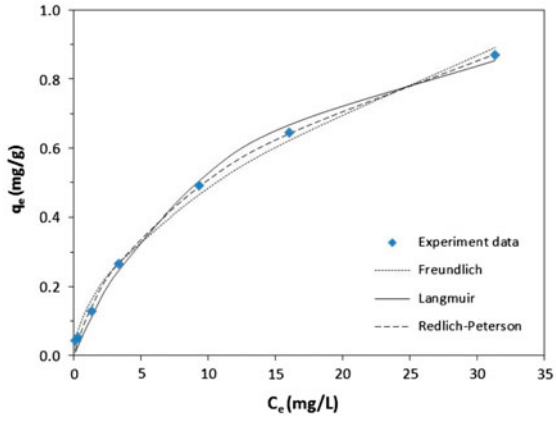

Fig. 5. Equilibrium isotherm model analysis. Model parameters are provided in Table 3.

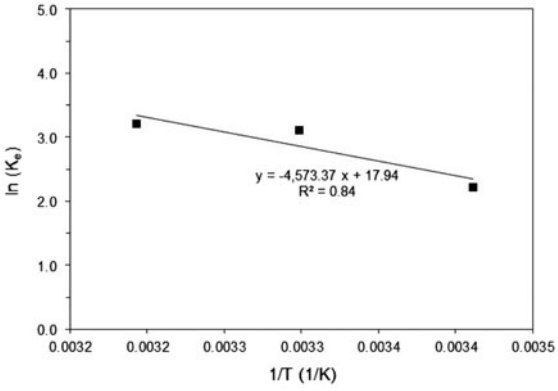

Fig. 6. Thermodynamic analysis for the removal of As(V) by functionalized ACF.

was determined to be 1.208 mg/g, which was lower than that of Zhang et al. [15], who reported the As(V) adsorption capacity of magnetite-doped ACF as 4.16 mg/g. This discrepancy could be attributed to the different experimental conditions between these two studies, including the adsorbent dose and As(V) concentration. Zhang et al. [15] performed the batch sorption experiments with the adsorbent (magnetite-doped ACF) dose of 0.7 g/L and As(V) concentration of 2 mg/L, whereas our batch experiments were done with the adsorbent dose of 20 g/L and As(V) concentration of 1 mg/L.

The reaction time data at different temperatures were used to perform the thermodynamic analysis using the following equations [23]:

$$\Delta G^{\circ} = \Delta H^{\circ} - T\Delta S^{\circ} \tag{12}$$

$$\Delta G^{\circ} = -\mathrm{RT}\ln(K_e) \tag{13}$$

$$\ln(K_e) = \frac{\Delta S^{\circ}}{R} - \frac{\Delta H^{\circ}}{\mathrm{RT}}; \quad K_e = \frac{\mathrm{aq}_e}{C_e} \tag{14}$$

where ΔG° is the change in Gibb's free energy, ΔS° is the change in entropy, ΔH° is the change in enthalpy, R is the gas constant (=8.314 J/mol/K), K_e is the equilibrium constant (dimensionless), and a is the adsorbent dose. The values of ΔS° and ΔH° were determined by plotting $\ln(K_e)$ vs. $1/T$ using Eq. (14), and the value of ΔG° was calculated from Eq. (12).

The thermodynamic data and analysis for As(V) sorption to functionalized ACF are presented in Fig. 6. The As(V) adsorption to functionalized ACF increased with increasing temperature from 20 to 40°C, demonstrating that the sorption process was endothermic.

The positive value of ΔH° (=38.02 kJ/mol) also indicated the endothermic nature of As(V) sorption. The positive value of ΔS° (=149.15 J/K/mol) showed that the randomness increased at the interface between the solid and solution during the sorption process. The negative values of ΔG° (20°C: –5.70; 30°C: –7.19; 40°C: –8.69 kJ/mol) indicated that the sorption process was spontaneous. Our results were similar to the report of Guo et al. [24], who showed the endothermic nature of As(V) removal by synthetic siderite ($FeCO_3$). Deliyanni et al. [25] also reported that the sorption of As(V) to synthetic akaganéite (β-FeOOH) nanocrystals was endothermic.

4. Conclusions

In this study, the removal of As(V) by functionalized ACF was examined. The batch experiments showed that the maximum adsorption capacity of As(V) in functionalized ACF was 1.208 mg/g. The adsorption of As(V) to functionalized ACF was sensitive to solution pH changes and decreased with an increase in the pH from 2.6 to 8.9. Kinetic model analysis showed that the pseudo-second-order model was the most suitable for describing the kinetic data. Equilibrium isotherm model analysis illustrated that the Redlich–Peterson model fitted well with the equilibrium data. Thermodynamic tests demonstrated that As(V) sorption to functionalized ACF increased with an increase in the temperature from 20 to 40°C, indicating the endothermic and spontaneous nature of the sorption process. This study demonstrated that the removal of As(V) by ACF could be enhanced via iron oxide impregnation.

Acknowledgments

This work was supported by the National Research Foundation of Korea, funded by the Ministry of Education, Republic of Korea (grant number 2014-027899).

References

[1] S. Dixit, J.G. Hering, Comparison of arsenic(V) and arsenic(III) sorption onto iron oxide minerals: Implications for arsenic mobility, Environ. Sci. Technol. 37 (2003) 4182–4189.
[2] J. Giménez, M. Martínez, D.J. Pablo, M. Rovira, L. Duro, Arsenic sorption onto natural hematite, magnetite, and goethite, J. Hazard. Mater. 141 (2007) 575–580.
[3] M. Suzuki, Activated carbon fiber: Fundamentals and applications, Carbon 32 (1994) 577–586.
[4] N.M. Osmond, Activated carbon fibre adsorbent materials, Adsorpt. Sci. Technol. 18 (2000) 529–539.
[5] Y.G. Ko, U.S. Choi, J.S. Kim, Y.S. Park, Novel synthesis and characterization of activated carbon fiber and dye adsorption modeling, Carbon 40 (2002) 2661–2672.
[6] K. Li, Y. Li, Z. Zheng, Kinetics and mechanism studies of p-nitroaniline adsorption on activated carbon fibers prepared from cotton stalk by $NH_4H_2PO_4$ activation and subsequent gasification with steam, J. Hazard. Mater. 178 (2010) 553–559.
[7] L. Zhang, L. Wan, N. Chang, J. Liu, C. Duan, Q. Zhou, X. Li, X. Wang, Removal of phosphate from water by activated carbon fiber loaded with lanthanum oxide, J. Hazard. Mater. 190 (2011) 848–855.
[8] S.J. Park, Y.S. Jang, Preparation and characterization of activated carbon fibers supported with silver metal for antibacterial behavior, J. Colloid Interface Sci. 261 (2003) 238–243.
[9] Q. Li, M.A. Page, B.J. Mariñas, K.S. Jian, Treatment of coliphage MS2 with palladium-modified nitrogen-doped titanium oxide photocatalyst illuminated by visible light, Environ. Sci. Technol. 42 (2008) 6148–6153.
[10] C. Chui, X. Quan, S. Chen, H. Zhao, Adsorption and electrocatalytic dechlorination of pentachlorophenol on palladium-loaded activated carbon fibers, Sep. Purif. Technol. 47 (2005) 73–79.
[11] J. Shi, J. Zheng, P. Wu, X. Ji, Immobilization of TiO_2 films on activated carbon fiber and their photocatalytic degradation properties for dye compounds with different molecular size, Catal. Commun. 9 (2008) 1846–1850.
[12] B.J. Kim, S.J. Park, Antibacterial behavior of transition-metals-decorated activated carbon fibers, J. Colloid Interface Sci. 325 (2008) 297–299.
[13] J. Liu, L. Wan, L. Zhang, Q. Zhou, Effect of pH, ionic strength, and temperature on the phosphate adsorption onto lanthanum-doped activated carbon fiber, J. Colloid Interface Sci. 364 (2011) 490–496.
[14] K.D. Hristovski, H. Nguyen, P.K. Westerhoff, Removal of arsenate and 17α-ethinyl estradiol (EE2) by iron (hydr)oxide modified activated carbon fibers, J. Environ. Sci. Health. Part A 44 (2009) 354–361.
[15] S. Zhang, X. Li, J.P. Chen, Preparation and evaluation of a magnetite-doped activated carbon fiber for enhanced arsenic removal, Carbon 48 (2010) 60–67.
[16] S. Zhang, X. Li, J.P. Chen, An XPS study for mechanisms of arsenate adsorption onto a magnetite-doped activated carbon fiber, J. Colloid Interface Sci. 343 (2010) 232–238.
[17] F.L. Mi, S.S. Shyu, S.T. Lee, T.B. Wong, Kinetic study of chitosan–tripolyphosphate complex reaction and acid-resistive properties of the chitosan–tripolyphosphate gel beads prepared by in-liquid curing method, J. Polym. Sci. Part B: Polym. Phys. 37 (1999) 1551–1564.
[18] M. Jarlbring, L. Gunneriusson, B. Hussmann, W. Forsling, Surface complex characteristics of synthetic maghemite and hematite in aqueous suspensions, J. Colloid Interface Sci. 285 (2005) 212–217.

[19] S.Y. Yoon, C.G. Lee, J.A. Park, J.H. Kim, S.B. Kim, S.H. Lee, J.W. Choi, Kinetic, equilibrium and thermodynamic studies for phosphate adsorption to magnetic iron oxide nanoparticles, Chem. Eng. J. 236 (2014) 341–347.
[20] S.S. Gupta, K.G. Bhattacharyya, Kinetics of adsorption of metal ions on inorganic materials: A review, Adv. Colloid Interface Sci. 162 (2011) 39–58.
[21] S.K. Bajpaia, M.K. Armob, Equilibrium sorption of hexavalent chromium from aqueous solution using iron(III)-loaded chitosan–magnetite nanocomposites as novel sorbent, J. Macromol. Sci. Part A 46 (2009) 510–520.
[22] K.Y. Foo, B.H. Hameed, Insights into the modeling of adsorption isotherm systems, Chem. Eng. J. 156 (2010) 2–10.
[23] A. Goswami, M.K. Purkait, Kinetic and equilibrium study for the fluoride adsorption using pyrophyllite, Sep. Sci. Technol. 46 (2011) 1797–1807.
[24] H. Guo, Y. Li, K. Zhao, Arsenate removal from aqueous solution using synthetic siderite, J. Hazard. Mater. 176 (2010) 174–180.
[25] E.A. Deliyanni, D.N. Bakoyannakis, A.I. Zouboulis, K.A. Matis, Sorption of As(V) ions by akaganéite-type nanocrystal, Chemosphere 50 (2003) 155–163.